

1 **Response to final editor comments**

2 **The authors would like to thank the editor for the continuation of valuable comments on**  
3 **the manuscript. We have responded to the specific comments below in bold.**

4 Comments to the Author:

5 The authors have addressed all the remaining concerns of the reviewers. There correction to the ERA-  
6 I has substantially changed the results, however, the change further strengthens the main results that  
7 SnowModel performance is superior, and so addresses the comment that, based on the previous  
8 assessment, ERA-I did as well as SnowModel in matching the in situ snow depth. Therefore, I judge  
9 that the manuscript should be accepted. There are two points that the change in ERA-I has made more  
10 clear to me, and I would recommend that some short additional discussion be added to clarify these.

11 1. In the prior revision, I made the following comment:

12 “One thing you did not point out is that snowmodel takes as its input precipitation from Polar-WRF,  
13 which will be different from ERA-I. So the comparison between ERA-I and snowmodel and in situ (at  
14 east for the CS-2 comparison) mostly just shows that the retrieval is sensitive to errors in snow depth,  
15 and not which method is necessarily better (snowmodel would presumably be better where, as you note,  
16 snow redistribution matters, but you have not shown that this is a factor here).”

17 To which you responded:

18 It is stated in the manuscript (L244-248 second version, L251-255 latest version) that hourly  
19 atmospheric forcing were generated by version 3.5 of the polar-optimized version of the Advanced  
20 Research Weather Research and Forecasting Model. The revised ERA-I dataset also now show that  
21 ERA-I is not suitable for retrieving sea ice thickness in this region at least.

22 Due to poor wording on my part, this misses my point. The point is that the precipitation fields from  
23 WRF-ARW that are used to drive SnowModel are not that same as ERA-I. In fact, I believe Polar WRF  
24 initialization and boundary conditions are provided by NCEP GFS (this may have changed) so that it  
25 also cannot be viewed as a downscaled model of ERA-I. This means that ERA-I performing poorly  
26 does not suggest that SnowModel is responsible for the much better fits. It could be that the WRF-ARW  
27 precipitation fields forcing SnowModel are much better and responsible for most of the improvement.  
28 The results do suggest that snow redistribution in SnowModel may be important, as the snow depth  
29 distribution from SnowModel matches in situ distribution much better than ERA-I (figure 3), but it is  
30 not clear if the high-resolution model WRF-ARW uses in this area actually produces similar spatial  
31 variation in precipitation that ERA-I cannot, nor whether the match to mean snow depth is due to  
32 SnowModel or primarily due to better precipitation in WRF-ARW.

33 This was not necessarily a goal of the study, and not raised by the reviewers, but I would suggest at  
34 least that some comment in the discussion about this point and its significance for the results would be  
35 helpful.

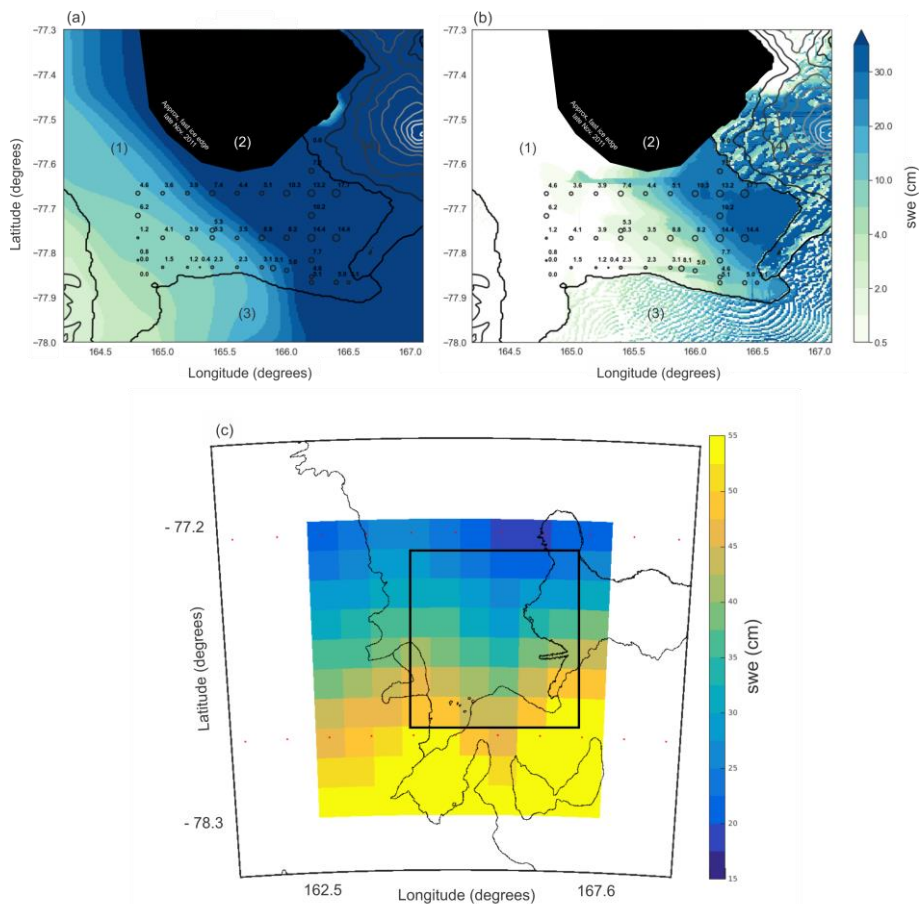
36 **Thank you for pointing this out, it is an important point to clarify. We have decided to include an**  
37 **additional plot in Figure 4 (Figure 4a) to showcase the importance of the SnowModel**  
38 **redistribution by wind.**

39

40

41

42



43  
 44 **Figure 4.** (a) MicroMet swe distribution (b) SnowModel swe distribution in McMurdo Sound, (1) fast  
 45 ice, (2) open water/pack ice, (3) McMurdo Ice Shelf, (4) Ross Island. The model swe distribution is the  
 46 mean of the simulation over the *in situ* measurement period (25th November-1<sup>st</sup> December). The *in situ*  
 47 measurements were converted to swe via the density measured at each site, if no measurement was  
 48 taken (21 sites) the average *in situ* snow density was used ( $385 \text{ kg m}^{-3}$ ). *In situ* measurement locations  
 49 are shown as black circles and are the mean of the 60 snow measurements taken at each site. The circle  
 50 sizes are weighted for swe to allow visualisation of the decreasing swe distribution from east to west.  
 51 Elevation contours are spaced at 400 m intervals; Mt Erebus (3,794 m) is the dominant topographic  
 52 feature on Ross Island to the east of the fast ice. (c) The interpolated 10 x 10 ERA-I grid with 1<sup>st</sup>  
 53 December accumulation total, the boundary of the SnowModel inset from (a) is shown as the black box.  
 54 The ERA-I centre points of the original grid are displayed as red dots.

55  
 56  
 57

58 We have also included the following in the text:

59 Section 4:

60 *“It is important to note the importance of redistribution by wind which is provided by SnowModel.*  
61 *The consequences of neglecting this influence on snow accumulation in the study region are clearly*  
62 *demonstrated in Figure 4. Figure 4a displays the accumulated precipitation from MicroMet, while*  
63 *this is built on in Figure 4b with the inclusion of the other SnowModel components. Over eastern*  
64 *areas of the study region, the MicroMet precipitation output as a standalone product provides swe*  
65 *values double that of the highest swe measured in situ. Although vastly improved, the general*  
66 *overestimation of swe by SnowModel is clearly visible in Figure 4b.”*

67 Section 6:

68 *“Without this model component included the precipitation provided by MicroMet (downscaled*  
69 *PWRF) provides very poor estimates of snow depth on sea.”*

70

71 2 In Figure 6, the cause of the range of the thicknesses is not clear, and not really discussed much in the  
72 manuscript. I can understand the range in ERA-I, since there is a large discrepancy here. But in the  
73 manuscript it is stated that SnowModel has a mean snow depth that is only 2 cm more (SWE, so ~5cm  
74 in snow depth) than in situ. Now, since equations 1-3 are all linear, I would have thought this offset  
75 ( $dTs \sim 5 \text{ cm}$ ) would cause an offset in the bounds shown by some modest amount (e.g.  $dTs * pw / (pw - pi)$ ,  
76 and  $dTs * (pw - ps) / (pw - pi)$  from the in situ bounds, or 30-50 cm). But in Figure 6 these changes are  
77 much greater (~ 1m). Also, since the Pd range shown would cover this ~5 cm bias, I do not understand  
78 why the range of the dots do not span the in situ depth indicated by the plus sign.

79 Either Figure 6 is showing something different, or I am not understanding how the bounds are being  
80 determined (is it showing the range of CS-2 derived thicknesses across the domain, and not the mean?  
81 Or possibly the 2 cm SWE bias is not scaled spatially, so the difference is mostly due to the larger bias  
82 in region 2?). It would be helpful to the reader for there to be a few sentences more explanation of what  
83 contributes to the differences in the results in Figure 6.

84 Figure 6 displays the mean sea ice thickness (which is representative of all valid CS-2 retrievals  
85 in the study region) for each month of the sea ice growth season. The grey dots are the thickness  
86 assuming the air-snow interface is considered freeboard, the blue dots the thickness if the snow-  
87 ice interface is considered freeboard. The other linear fits between them represent the trends  
88 assuming different penetration factors. The large range in thickness through these different  
89 assumptions is because of the snow depth. ERA-I has the largest snow depth followed by  
90 SnowModel, followed by AMSR-E and the results reflect this. The bias is not scaled spatially and  
91 you are correct that the larger snow depths in regions 2 and 3 are driving the range in resultant  
92 thicknesses which also account for why the large penetration factors still do not meet the in situ  
93 thickness in Fig 5a. Fig 4b shows the high swe values which are in excess of 10 cm swe (30 cm +  
94 snow depth) for over half of area in fastening areas 2 and 3. In the very eastern areas values are  
95 as high as 100 cm of snow.

96 The forcing of this range is covered by the following *“From equations 1-3, sea ice thickness is*  
97 *highly sensitive to the snow-ice ratio for the measured freeboard. This results in a large range in sea*  
98 *ice thickness for all snow products through the growth season (Fig. 5). This range in inferred*  
99 *thickness is driven by the amount of snow produced by the models as Eq. 1 and Eq. 2 subtract and*  
100 *add the product of this value in their second terms respectively. As the snow depth increases, in some*  
101 *cases to higher values than the measured freeboard the Pd simply provides a correcting factor for*  
102 *this discrepancy.”* in section 5.

103 **To provide clarity on the specific point mentioned above, the following sentences have been**  
104 **included in section 5:**

105 *“The ranges in sea ice thickness estimated with SnowModel as the snow depth input are substantially*  
106 *smaller than ERA-I (Fig. 5), but still have a larger range than the mean discrepancy from in situ*  
107 *measurements might suggest (Fig. 2). This is driven by CS-2 retrievals over the eastern areas of*  
108 *fastening areas 2 and 3 where swe values are high, especially towards the end of the growth season*  
109 *(Fig. 4b).”*

110 Other minor comments:

111 Line 532-543, page 17. To clarify, ASPECT is from shipboard underway observations. These do not  
112 necessarily avoid ridged areas, but the estimated snow depths are probably somewhat biased as they are  
113 often estimated based on the snow depth on the level ice portion of the ice, and perhaps less from ridged  
114 areas, and the ship likely does avoid heavily ridged, thick ice.

115 **To avoid confusion, sentence amended to “Vessels are restricted in their ability to sample in heavily**  
116 **deformed and thicker sea ice areas where the snow is typically higher. Because of this, it is postulated**  
117 **that shipborne observations of in situ snow thickness were biased low in comparison to AMSR-E**  
118 **snow depth.”**

119 Line 605, page 19 – confidently, not confidentially

120 **Amended.**

121

122

123

124

125

126

127

128

129

130

131

132

133

134

135

136

137

138

139 Snow driven uncertainty in CryoSat-2 derived Antarctic sea ice thickness -  
140 insights from McMurdo Sound

141

142 Daniel Price<sup>1</sup>, Iman Soltanzadeh<sup>2</sup> & Wolfgang Rack<sup>1</sup>, Ethan Dale<sup>3</sup>

143 <sup>1</sup>Gateway Antarctica, University of Canterbury, Private Bag 4800, Christchurch, New Zealand

144 <sup>2</sup>Met Service, 30 Salamanca Road, Kelburn, Wellington, 6012, New Zealand

145 <sup>3</sup>Department of Physics and Astronomy, University of Canterbury, Christchurch, New Zealand

146 Correspondence to: Daniel Price (daniel.price@canterbury.ac.nz)

147 **Abstract.** Knowledge of the snow depth distribution on Antarctic sea ice is poor but is critical to  
148 obtaining sea ice thickness from satellite altimetry measurements of freeboard. We examine the  
149 usefulness of various snow products to provide snow depth information over Antarctic fast ice in  
150 McMurdo Sound with a focus on a novel approach using a high-resolution numerical snow  
151 accumulation model (SnowModel). We compare this model to results from ECMWF ERA-Interim  
152 precipitation, EOS Aqua AMSR-E passive microwave snow depths and *in situ* measurements at the end  
153 of the sea ice growth season in 2011. The fast ice was segmented into three areas by fastening date and  
154 the onset of snow accumulation was calibrated to these dates. SnowModel captures the spatial snow  
155 distribution gradient in McMurdo Sound and falls within 2 cm snow water equivalent (swe) of *in situ*  
156 measurements across the entire study area. However, it exhibits deviations of 5 cm swe from these  
157 measurements in the east where the effect of local topographic features has caused an overestimate of  
158 snow depth in the model. AMSR-E provides swe values half that of SnowModel for the majority of the  
159 sea ice growth season. The coarser resolution ERA-Interim, produces a very high mean swe value 20  
160 cm higher than *in situ* measurements. These various snow datasets and *in situ* information are used to  
161 infer sea ice thickness in combination with CryoSat-2 (CS-2) freeboard data. CS-2 is capable of  
162 capturing the seasonal trend of sea ice freeboard growth but thickness results are highly dependent on  
163 what interface the retracked CS-2 height is assumed to represent. Because of this ambiguity we vary  
164 the proportion of ice and snow that represents freeboard – a mathematical alteration of the radar  
165 penetration into the snow cover and assess this uncertainty in McMurdo Sound. The range in sea ice  
166 thickness uncertainty within these bounds, as means of the entire growth season are 1.08 m, 4.94 m and  
167 1.03 m for SnowModel, ERA-Interim and AMSR-E respectively. Using an interpolated *in situ* snow  
168 dataset we find the best agreement between CS-2 derived and *in situ* thickness when this interface is  
169 assumed to be 0.07 m below the snow surface.

170 **1 Introduction**

171 The knowledge of Antarctic sea ice extent, area, drift and roughness have been greatly  
172 improved over the last forty years, principally supported by satellite remote sensing.  
173 Nevertheless, many knowledge gaps remain which restrict our ability to better understand the  
174 Antarctic sea ice system. A foremost concern is inadequate data for the snow depth distribution  
175 on Antarctic sea ice (Pope et al., 2016) as the presence of snow has many important  
176 implications for the sea ice cover (Massom et al., 2001, Wu et al., 1999, Fichfet and Maqueda,  
177 1999). The thermal conductivity of snow is almost an order of magnitude less than sea ice  
178 (Maykut and Untersteiner, 1971) and as snow accumulates, it reduces the conductive heat flux  
179 from the ocean to the atmosphere, slowing growth rates, but also leads to thickening of the ice  
180 cover through snow-ice formation (Maksym and Markus, 2008). Snow significantly increases  
181 the albedo of the sea ice cover and in the austral spring and summer snow melt drives fresh  
182 water input to the Southern Ocean (Massom et al., 2001). Perhaps most crucially from a satellite  
183 observation perspective, our inability to accurately monitor its depth and distribution causes  
184 large uncertainty when estimating sea ice thickness. Sea ice thickness measurements as inferred

185 via satellite freeboard estimates (Schwegmann et al., 2016, Kurtz and Markus, 2012, Giles et  
186 al., 2008) currently present the the best opportunity to establish yet unpublished datasets on  
187 decadal trends in Antarctic sea ice volume. Without improved snow depth measurements, it is  
188 impossible to discern meaningful trends in Antarctic sea ice thickness. Errors are introduced to  
189 thickness estimates via the snow cover for two principal reasons:

- 190 1. Snow depth information is inaccurate/not available and therefore the ratio of ice  
191 and snow above the waterline is poorly quantified or unknown.
- 192 2. Uncertainty about what surface the retracking point on the radar waveform actually  
193 represents between the ice freeboard and snow freeboard. This initial measurement  
194 is commonly referred to as radar freeboard.

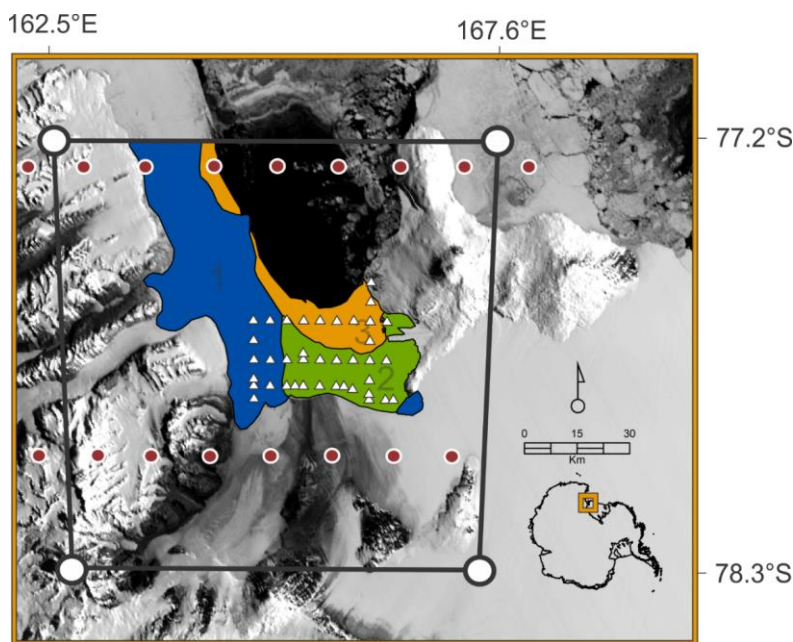
195 The uncertainty associated with these two factors has not been directly investigated using  
196 satellite altimeter information over Antarctic sea ice. This work provides insights from a case  
197 study region, McMurdo Sound Antarctica. Snow on Arctic sea ice has been investigated in  
198 more detail and over a longer period than the Antarctic so climatologies can be produced  
199 (Warren et al., 1999). These datasets in combination with satellite altimetry, and suitable  
200 airborne investigations have permitted the completion of pan-Arctic thickness assessments  
201 (Kurtz et al., 2014, Laxon et al., 2013, Kwok and Cunningham, 2008). The research community  
202 lacks snow climatology information in the Southern Ocean, though dedicated basin-scale snow  
203 depth assessments are available via passive microwave sensors (Markus and Cavalieri, 2006).  
204 Continual improvements in our monitoring ability are key to support the current ESA satellite  
205 altimeter missions, CryoSat-2 (CS-2) and Sentinel-3 and NASA's laser altimeter mission  
206 ICESat-2. To date only AMSR-E passive microwave data have been used in combination with  
207 altimetry to estimate sea ice thickness. The AMSR-E algorithm's accuracy is decreased by  
208 rough sea ice and deep and complex snow (Kern and Ozsoy-Çiçek, 2016, Kern et al., 2011,  
209 Worby et al., 2008b, Stroeve et al., 2006), both typical characteristics of the Antarctic sea ice  
210 cover. Using laser altimetry, some investigators have assumed zero ice freeboard (Kurtz and  
211 Markus, 2012), that is, the snow loading forces the ice surface to the waterline, negating the  
212 need for snow depth data. Thickness estimates using this approach are likely biased low and  
213 although this simplification provides valuable insights, it does not provide sea ice thickness at  
214 the desired accuracy. This work is motivated by the necessity for a comprehensive  
215 understanding of the usefulness of snow products in the Southern Ocean, and the need to  
216 investigate new avenues for producing snow depth products over Antarctic sea ice. Here we  
217 make use of a detailed *in situ* dataset to assess modelling and satellite approaches to construct  
218 snow depth over the 2011 sea ice growth season. In a first attempt over Antarctic fast ice, using  
219 a high-resolution snow accumulation model called SnowModel (Liston and Elder, 2006a) and  
220 synthetic aperture radar imagery, we are able to establish when the sea ice fastens and  
221 accumulate snow from those dates for three areas of fast ice in McMurdo Sound in the south-  
222 western Ross Sea. The high-resolution model results are compared to snow products from two  
223 other independent datasets, the first ERA-Interim (ERA-I) precipitation and the second satellite  
224 passive microwave snow depth from AMSR-E. With these different snow depth datasets we  
225 infer sea ice thickness via freeboard measurements from CS-2. The interaction of radar energy  
226 with the snow pack is highly complex and here we take a simplified approach given the surface  
227 height has already been established by the ESA retracking procedure. Given the uncertainty of  
228 the position of the retracking point with reference to the height above sea level, we assume

229 different penetration depths into the snowpack by varying the proportion of ice and snow that  
230 represents freeboard. We compare the inferred CS-2 thicknesses with *in situ* information.

## 231 2 Study area, field and satellite data

### 232 2.1 McMurdo Sound and field data

233 A detailed *in situ* sea ice measurement campaign was carried out in November 2011 on the fast  
234 ice in McMurdo Sound (Fig. 1). This involved sea ice thickness, freeboard and snow  
235 depth/snow density measurements at 39 sites. Freeboard was measured 5 times in a cross  
236 profile at each site, once at the centre of the cross and once at the terminus of each line, as was  
237 thickness. Mean snow depths for each *in situ* site represent 60 individual snow depth  
238 measurements over that same cross-profile at 50 cm intervals. Snow density was measured at  
239 18 sites, well distributed across the area, the mean of these sites is used for this analysis unless  
240 stated otherwise. A full overview of the measurement procedure is provided in Price et al.  
241 (2014). Additional *in situ* measurements of sea ice thickness are included in the analysis, two  
242 measurements taken at one location in McMurdo Sound in July and November. Assuming a  
243 constant growth rate between these measurements they are used in section 5 as a comparison  
244 to CS-2 inferred sea ice growth rates. More detail on how the *in situ* thickness measurements  
245 are used and how they should be interpreted is provided in section 5.



246  
247 **Figure 1.** McMurdo Sound study area with each fastening area as identified by Envisat radar imagery:  
248 area 1 – 01/04/2011 (Blue), area 2 – 29/04/2011 (Green), area 3 – 01/06/2011 (Orange) and SnowModel  
249 domain bounded by the black box. Fastening areas are superimposed on a MODIS image acquired on  
250 15 November at the time of maximum fast ice extent in 2011. The locations of 39 measurement sites  
251 used to produce the *in situ* snow and sea ice statistics are shown as white triangles. The centre points of  
252 each ERA-I 0.75° x 0.75° grid cell in the vicinity of the study area are displayed as red circles.

253 **2.2 Envisat**

254 The sea ice freeze-up provides a point from which snow can begin to accumulate on the sea ice  
255 surface. Freeze-up could be identified using passive microwave information, but this data does  
256 not provide the spatial resolution to segment the sea ice area appropriately for SnowModel's  
257 200 m resolution. In McMurdo Sound during the freeze-up period, pack ice is generally  
258 advected north out of the study area unless it fastens. In addition to floe movement, before  
259 fastening occurs, snowfall is subject to uncertainty from flooding events and snow loss to leads,  
260 influences on the eventual snow depth that we have no way of accurately monitoring. With the  
261 resolution restriction in mind and these uncertainties, we have selected the sea ice fastening  
262 date to begin snow accumulation. To identify the dates and the pattern in which the sea ice  
263 fastens across the study area, we use a string of C-band Advanced Synthetic Aperture Radar  
264 (ASAR) images from Envisat acquired in Wide Swath mode. We process these files using  
265 GAMMA Software to produce ASAR imagery with a spatial resolution of 150 x 150 m. By  
266 comparing motion and patterns between sequential images we are able to identify three areas  
267 that fastened independently of one another. The first area of fast ice was established by 1 April  
268 (area 1 – Fig. 1), by the end of April, a second area of fast ice had formed along the southern  
269 extremity of the Sound (area 2 – Fig. 1), and by the beginning of June, a third area had fastened  
270 (area 3 – Fig. 1). The largest gap in the Envisat image string is 8 days but no large gaps are  
271 found around key fastening dates. The typical spacing is 1-2 days so we have confidence we  
272 have reduced our error in the fastening date to less than 2 days. These three areas persisted for  
273 the winter and when combined, made up the fast ice area present in late November when *in*  
274 *situ* measurements were made.

275 **2.3 AMSR-E**

276 The EOS Aqua Advanced Microwave Scanning Radiometer (AMSR-E) was operational from  
277 December 2002 until 4 October 2011. The snow depth product provided by NSIDC  
278 ([https://nsidc.org/data/AE\\_SI12/versions/3#](https://nsidc.org/data/AE_SI12/versions/3#)) is provided at a 12.5 x 12.5 km<sup>2</sup> polar  
279 stereographic projection and reported as a 5-day running mean, that mean inclusive of that day  
280 and the prior 4 days. We remove data where ice concentrations are lower than 20%. Gridded  
281 snow depth values are calculated using the spectral gradient ratio of the 18.7 and 36.5 GHz  
282 vertical polarisation channels. For snow free sea ice the emissivity is similar for both  
283 frequencies. Snow depth increases attenuation from scattering but is more pronounced at 36.5  
284 GHz than at 18.7 GHz, resulting in higher brightness temperatures at 18.7 GHz (Comiso et al.,  
285 2003, Markus and Cavalieri, 1998). Using coefficients derived from a linear regression of *in*  
286 *situ* snow depth measurements on microwave data, and a 36.5-18.7 GHz ratio corrected for sea  
287 ice concentration, snow depth can be estimated (Comiso et al., 2003). Snow depth retrievals  
288 are restricted to dry snow only and to a depth of less than 50 cm. Variable snow properties  
289 including snow grain size, snow density and liquid water content influence microwave  
290 emissivity from the sea ice surface and the algorithm is reported to have a precision of 5 cm  
291 (Comiso et al., 2003) . Given the extreme southern latitude of the study area, snow conditions  
292 throughout this study were very dry, supported by snow pit analysis on the sea ice in November  
293 with no wet snow or lensing observed. AMSR-E cells are included in the analysis if over 50%  
294 of the cell lies within the fast ice mask, and segmented into each fastening area by that same  
295 criteria. 22 AMSR-E cells are used and due to the instrument failure in early October 2011,  
296 data for the last two months of this investigation are unavailable.



## 297 2.4 CryoSat-2

298 CS-2 was launched in 2010 and houses a *Ku*-band radar altimeter (centre frequency 13.6 GHz).  
299 The altimeter has an approximate footprint size of 380 m x 1560 m and samples along-track at  
300 300 m intervals. The instrument has three modes and over the coastal Antarctic operates its  
301 interferometric (SIN) mode. This mode uses both of the satellite's antennas to identify the  
302 location of off-nadir returns accurately. This is not the dedicated sea ice mode, but it is still  
303 suitable for sea ice freeboard retrieval (Price et al., 2015; Armitage and Davidson, 2014). In  
304 section 5, to assess the usefulness of the evaluated snow products, we infer sea ice thickness  
305 from CS-2 freeboard measurements.

306 The ESA L2 baseline C SIN mode (SIR\_SIN\_L2 – available at: [http://science-](http://science-pds.cryosat.esa.int/)  
307 [pds.cryosat.esa.int/](http://science-pds.cryosat.esa.int/)) data set provides a retracked height for the surface over sea ice and this  
308 initial measurement is termed radar freeboard. The processing closely follows that described  
309 in Price et al. (2015), but to reduce noise, two modifications are made to achieve more detailed  
310 scrutiny of the CS-2 height retrievals. The first is a more stringent exclusion of off-nadir  
311 elevation retrievals, the threshold is halved from  $\pm 750$  m to  $\pm 375$  m; data located at greater  
312 distances from nadir are discarded. The second is the rejection of freeboard measurements of  
313 less than -0.24 m and greater than 0.74 m. Following Schwegmann et al (2016) the  $\pm 0.24$  m  
314 accounts for speckle range noise in the CS-2 data and the + 0.5 m threshold additionally  
315 incorporates an expected maximum sea ice freeboard of 0.5 m for fast ice in McMurdo Sound  
316 (as measured *in situ* in 2011). Each CS-2 radar freeboard measurement is cross-referenced to  
317 fastening areas 1, 2 and 3 and assigned a snow depth ( $T_s$ ) value from the described snow  
318 products. From the ESA retracked product there is currently no consensus on what surface the  
319 radar freeboard represents over sea ice, the air-snow interface, the snow-ice interface or an  
320 undefined interface between the two. Laboratory experiments (Beaven et al., 1995) and  
321 comparisons of other radar altimeter systems with *in situ* measurements (Laxon et al., 2003)  
322 suggest the snow-ice interface is detected. It is clear that the presence of snow influences the  
323 CS-2 height retrieval, but precisely how, is dependent on the surface roughness (Kurtz et al.,  
324 2014; Hendricks et al., 2010; Drinkwater, 1991), its depth (Kwok, 2014) and its dielectric  
325 properties (Hallikainen et al., 1986). The mean depth of the dominant backscattering surface  
326 measured using a surface based *Ku*-band radar over snow covered Antarctic sea ice was around  
327 50% of the mean measured snow depth, and the snow-ice interface only dominated when  
328 morphological features or flooding were absent (Willatt et al., 2010). Wingham et al. (2006)  
329 indicate the snow-ice interface is represented by the ESA retracked height. No other  
330 information is available about the assumptions made here, only that for diffuse echoes in SAR  
331 processing, for baseline C, a new retracker was implemented (Bouffard, 2015). It is unclear  
332 what the original retracking assumptions are for any retrieval mode and if any changes were  
333 made to SIN mode for baseline C. A prior study of CS-2 waveform behaviour over the same  
334 study area found ESA L2 freeboard to be located between the air-snow and snow-ice interface  
335 (Price et al., 2015). Given this uncertainty we apply a simple methodology to discover the range  
336 of thicknesses as inferred via this CS-2 data. We explore this possible range by changing the  
337 amount of snow and ice assumed to represent the freeboard measurement in the thickness  
338 equation. There is no physical change to the actual radar penetration, the inferred thickness is  
339 simply altered mathematically using a varying penetration depth ( $Pd$ ) into the snow pack.  
340 Equation 1 assumes that the snow surface is detected, equation 2 that the sea ice surface is  
341 detected and equation 3 that an arbitrary surface at varying  $Pd$  values into the snow pack (0.02

342 m, 0.05 m, 0.10 m, 0.15 m, 0.30 m and 0.50 m - or to the snow-ice interface, whichever criteria  
 343 is met first) represents the retracking point. The radar freeboard is corrected when snow is  
 344 present and penetration is assumed (i.e.  $Pd > 0$ ) for the reduction of the speed of the radar wave  
 345 through the snow pack following the procedure described in Kurtz et al (2014). We derive sea  
 346 ice thickness ( $T_i$ ) using the newly corrected freeboard ( $Fb$ ) and the described equations;

347

$$348 \quad T_i = \frac{\rho_w}{\rho_w - \rho_i} Fb - \frac{\rho_w - \rho_s}{\rho_w - \rho_i} T_s \quad (1)$$

349

$$350 \quad T_i = \frac{\rho_w}{\rho_w - \rho_i} Fb + \frac{\rho_s}{\rho_w - \rho_i} T_s \quad (2)$$

351

$$352 \quad T_i = \frac{\rho_w}{\rho_w - \rho_i} Fb - \frac{\rho_w - \rho_s}{\rho_w - \rho_i} T_s + \frac{\rho_w}{\rho_w - \rho_i} Pd \quad (3)$$

353

354 where  $\rho_w$  ( $1027 \text{ kgm}^{-3}$ ),  $\rho_i$  ( $925 \text{ kgm}^{-3}$ ) and  $\rho_s$  ( $385 \text{ kgm}^{-3}$ ) are the densities of water, sea ice and  
 355 snow respectively.  $\rho_w$  is informed by an unpublished time series of surface salinity  
 356 measurements taken from October 2008 to October 2009 along the front of the McMurdo Ice  
 357 Shelf. The range in  $\rho_w$  during this period is less than  $1 \text{ kgm}^{-3}$ . The  $\rho_i$  value used here is in the  
 358 middle of the measured range in McMurdo Sound, the use of which is discussed in Price et al.  
 359 (2014).  $\rho_s$  is the mean value taken from 18 of the 39 *in situ* sites where snow density was  
 360 measured.

### 361 **3 Atmospheric models for snow accumulation**

#### 362 **3.1 High resolution model**

363 SnowModel is a numerical modelling system with four main components: (1) MicroMet, a  
 364 quasi-physically-based, high-resolution meteorological distribution model (Liston and Elder,  
 365 2006b) (2) Enbal, a surface energy balance and snowmelt model (Liston et al., 1999) (3)  
 366 SnowTran-3D, a wind driven snow redistribution routine (Liston et al., 2007, Liston and Sturm,  
 367 1998) and (4) SnowPack, a multilayer snow depth and water-equivalent model (Liston and  
 368 Sturm, 1998). The main objective of MicroMet is to provide seamless atmospheric forcing  
 369 data, both temporally and spatially to the other SnowModel components. MicroMet is capable  
 370 of downscaling the fundamental atmospheric forcing such as air temperature, relative humidity,  
 371 wind speed, wind direction, incoming solar radiation, incoming longwave radiation, surface  
 372 pressure, and precipitation. Other SnowModel submodels simulate surface energy balance, and  
 373 moisture exchanges including snow melt, snow redistribution and sublimation. SnowModel  
 374 also incorporates multilayer heat and mass-transfer processes within the snow (e.g. snow  
 375 density evolution).

376 SnowModel is capable of initializing with both *in situ* and gridded model data and has been  
 377 evaluated in many geographical locations including Greenland and Antarctica (Liston and  
 378 Hiemstra, 2011; Liston and Hiemstra, 2008; Liston and Winther, 2005; Mernild et al., 2006).  
 379 To the authors knowledge, and at the time of writing this is only the second application of  
 380 SnowModel in a sea ice environment. Liston et al. (2018) applied SnowModel with an

381 additional component that accounted for snowdrifts and snow dunes, at very high spatial  
382 resolution over Arctic sea ice with positive results.

383 SnowModel requires topography, land cover and various atmospheric forcing. The minimum  
384 meteorological requirements of the model are near-surface air temperature, precipitation,  
385 relative humidity, wind speed and direction data from Automatic Weather Stations (AWS)  
386 and/or gridded numerical models. Determining the influence of wind and other atmospheric  
387 forcing on snow distribution in a complex terrain requires the use of numerical atmospheric  
388 models. Many studies have demonstrated that high-resolution models are vital for simulating  
389 topographic and land-use impacts on wind, hydraulic jump and associated turbulence (Olafsson  
390 and Agustsson, 2009; Agustsson and Olafsson, 2007). For this research, hourly atmospheric  
391 forcing were generated by version 3.5 of the polar-optimized version of the Advanced Research  
392 Weather Research and Forecasting Model (WRF-ARW; Skamarock et al., 2008) known as  
393 Polar WRF (Bromwich et al., 2009) or PWRF (<http://polarmet.osu.edu/PWRF>) at 3 km  
394 horizontal resolution.

395 The WRF-ARW (hereafter, WRF) is a state-of-the-art model that is equipped with a fully  
396 compressible, Eulerian and nonhydrostatic dynamic core. This model uses Arakawa C-grid  
397 staggering in the horizontal and utilises a mass terrain-following coordinate vertically. Several  
398 physical parameterization schemes are available in WRF, and some of those used for this work  
399 are described below. The WRF single-moment 6-class microphysics scheme (WSM6; (Hong  
400 and Lim, 2006)) is a cloud microphysics scheme, which includes various water phases  
401 including graupel. This likely improves precipitation and cloud related predictions at higher  
402 spatial resolution. For radiation, the rapid radiative transfer model (RRTM;(Mlawer et al.,  
403 1997)) and the empirically based Dudhia short-wave radiation scheme (Dudhia, 1989) are used  
404 as the long and short wave radiation schemes, respectively. The Mellor–Yamada–Nakanishi–  
405 Niino (MYNN; Nakanishi and Niino, 2006, Nakanishi and Niino, 2004, Nakanishi, 2001)  
406 level-2.5 scheme is used to take into account subgrid-scale turbulent fluxes.

407 The Noah LSM (Chen and Dudhia, 2001) with four soil layers, which is able to handle sea-ice  
408 and polar conditions through modifications described below was chosen as the land surface  
409 model. Generally, mesoscale numerical models including WRF have simple representations  
410 for sea ice thickness and snow depth on sea ice. This shortcoming leads to an outstanding error  
411 in the simulation of the snow and mass balance in the polar regions. To address this issue,  
412 PWRF improved the representation of heat fluxes through snow and ice in the Noah LSM.  
413 Further, this version of PWRF modified sea ice and snow albedos and made it accessible to  
414 define spatially varying sea ice thickness and snow depth on sea ice [for further detailed  
415 information about PWRF see Hines et al. (2015)].

416 The models, PWRF and SnowModel are coupled in an off-line manner. This means that the  
417 PWRF model ran for the entire study period first, then SnowModel initiated based on the  
418 PWRF simulated atmospheric forcing and there is no feedback from SnowModel to the  
419 atmospheric model. In order to increase the spatial resolution of the PWRF outputs, before  
420 ingesting the atmospheric forcing to the SnowModel, PWRF gridded data are interpolated to a  
421 new grid, and then corrected physically according to topography using the MicroMet  
422 submodel. The spatial resolution of SnowModel is 200 m and its output is segmented into sea  
423 ice fastening areas as indicated by the Envisat imagery (Fig. 1). Model outputs are reported as  
424 hourly means beginning at 00:00 1st April 2011 and ending at 00:00 1st December 2011.

425 SnowModel outputs snow depth and swe. The model has a varying density over time. The swe  
426 output is important as it allows comparison of the model to the other snow products which have  
427 different density assumptions.

### 428 **3.2 Low resolution model**

429 ERA-I is a global atmospheric reanalysis product on a  $0.75^\circ \times 0.75^\circ$  grid available from 1  
430 January 1989 (Dee et al., 2011). Precipitation data (mm water equivalent) are available at three  
431 hourly intervals and are converted to snow depth when required using the average snow density  
432 of  $385 \text{ kgm}^{-3}$  measured *in situ* in 2011. Using splines we interpolate the coarse resolution ERA-  
433 I grid and provide a  $10 \times 10$  grid over the study area with a cell resolution of 12 km. The  
434 reanalysis does not account for snow transport but with the interpolated grid we are able to  
435 segment the model for sea ice fastening dates and begin snow accumulation at the correct time.  
436 We average the three hourly outputs, the reported ERA-I data are daily averages for each  
437 fastening area.

### 438 **4 Snow product evaluation**

439 When the three snow products are compared to one another, or to *in situ* measurements, all  
440 snow depths are reduced to snow water equivalent (swe) via their respective densities to  
441 remove any bias associated with varying density between snow datasets. SnowModel provides  
442 a swe output via a time varying snow density during the model run, AMSR-E snow depths are  
443 reduced to swe using average *in situ* measured snow density in November, and ERA-I  
444 precipitation is provided as swe in its original format. The SnowModel evaluation is split into  
445 three parts, firstly, an accumulation time-series is presented for each snow product segmented  
446 by each fastening area, and this time series is the mean snow depth for each product within  
447 each area (Fig. 2). Secondly, selected SnowModel grid cells are directly compared to spatially  
448 coincident *in situ* measurement sites in November (Fig. 3) and thirdly, the SnowModel and  
449 ERA-I distributions are plotted as maps at the end of the model run for spatial comparison (Fig.  
450 4). The model swe values used for direct comparison to *in situ* measurements in Figures 3 and  
451 4 are the mean at each site between 25<sup>th</sup> November and 1<sup>st</sup> December, the period over which *in*  
452 *situ* measurements were made.

453 The SnowModel mean swe for all areas at the end of the simulation is 2 cm higher than *in situ*  
454 swe mean. However, SnowModel clearly presents two very different snow accumulation  
455 patterns, one in the west covering area 1 and one in the east covering areas 2 and 3. Mean swe  
456 values in area 1 reach a maximum of 2 cm during the 8-month study period while in areas 2  
457 and 3 they are in excess of 10 cm. This broad spatial distribution produced by SnowModel  
458 compares well with *in situ* measurements and general observations in November 2011, which  
459 recorded an increasing gradient in snow depth from west to east (Fig. 4). However, when each  
460 fastening area is directly compared to *in situ* means for those areas, swe is underestimated in  
461 area 1 ( $2 \text{ cm} < \textit{in situ}$ ), slightly overestimated in area 3 ( $1 \text{ cm} > \textit{in situ}$ ) and substantially  
462 overestimated in area 2 ( $5 \text{ cm} > \textit{in situ}$ ) (Fig. 2). Only modelled swe in area 3 falls within the  
463 standard deviation of the *in situ* mean. In the east, snow depth increases are noted in mid-May,  
464 mid-June, early-July, early and mid-August and late-September. The snow depth evolution in  
465 the west of the Sound over area 1 follows a separate pattern with negligible increases in mid/late  
466 April, mid-May, mid-July, late-September and early-November. When coincident pixels are  
467 directly compared to *in situ* data with coincident pixels SnowModel overestimates swe in the  
468 study area and therefore the model has better agreement with *in situ* maximum values ( $r^2 =$

469 0.56) than with the mean ( $r^2 = 0.53$ ) or minimum ( $r^2 = 0.30$ ) values (Fig. 3). It is important to  
470 note the importance of redistribution by wind which is provided by SnowModel. The  
471 consequences of neglecting this influence on snow accumulation in the study region are clearly  
472 demonstrated in Figure 4. Figure 4a displays the accumulated precipitation from MicroMet,  
473 while this is built on in Figure 4b with the inclusion of the other SnowModel components. Over  
474 eastern areas of the study region, the MicroMet precipitation output as a standalone product  
475 provides swe values double that of the highest swe measured *in situ*. Although vastly improved,  
476 the general overestimation of swe by SnowModel is clearly visible in Figure 4b. Values in the  
477 eastern most section of the sea ice cover in McMurdo Sound, adjacent to Ross Island are in the  
478 order of 20 to 35 cm swe. These values are all larger than the highest *in situ* measured swe of  
479 17.7 cm and for large areas, they still remain over double the measured value. In the central  
480 area of the Sound, modelled swe decreases in agreement with measured swe with 5 *in situ* sites  
481 agreeing within  $\pm 0.5$  cm of SnowModel swe (Fig. 3 and Fig. 4b). The western region of sea  
482 ice in fastening area 1 has far less measured snow. The model produces this well but values are  
483 too low. The extremes, where there is a lot of snow and where there is very little snow both  
484 seem to be exaggerated by the model.

485 Unlike SnowModel or the *in situ* distribution in late November AMSR-E swe follows a similar  
486 pattern over time in all fastening areas. For areas 2 and 3, May through June, AMSR-E and  
487 SnowModel produce similar swe values, agreeing within 1.5 cm in areas 2 and 3. In area 1  
488 AMSR-E swe fluctuates but is typically about 2.5-3 cm higher than SnowModel. As the growth  
489 season progresses AMSR-E remains significantly lower than SnowModel swe in areas 2 and  
490 3, by up to 10 cm. swe values are higher in area 2 than area 3 in agreement with SnowModel.  
491 However, in area 1 swe values are four times larger than SnowModel. Most importantly, the  
492 longitudinal swe gradient indicated by SnowModel and supported by *in situ* data is opposite  
493 when measured using AMSR-E (i.e. swe is higher in the west than in the east for the duration  
494 of the times series). As the AMSR-E instrument failed in early October, we are unable to  
495 validate it with *in situ* measurements. ERA-I also produces a different snow distribution to  
496 SnowModel and *in situ* data (Fig. 4c) with an area of lower swe values in the central area of  
497 the fast ice and higher swe values over the western and eastern areas. The mean deviation over  
498 the entire study area from *in situ* measurements is 20 cm swe. ERA-I swe values are over  
499 double that of SnowModel for areas 2 and 3 and an order of magnitude higher for area 1 (Fig.  
500 2). The ERA-I temporal snowfall pattern is the same between all areas and is similar to that  
501 produced by Snow Model in areas 2 and 3.

502

503

504

505

506

507

508

509

**Commented [DP1]:** Additional comments about the importance of redistribution by wind provided by SnowModel as opposed to the standalone downscaled PRWF input but MicroMet.

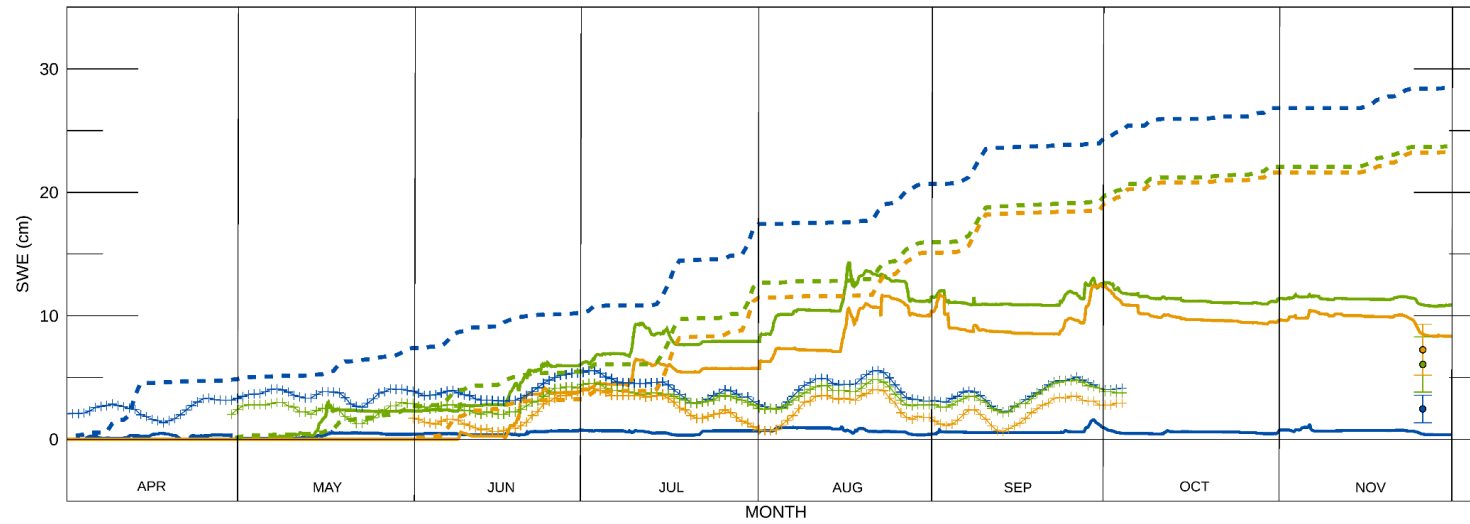
510

511

512

513

514

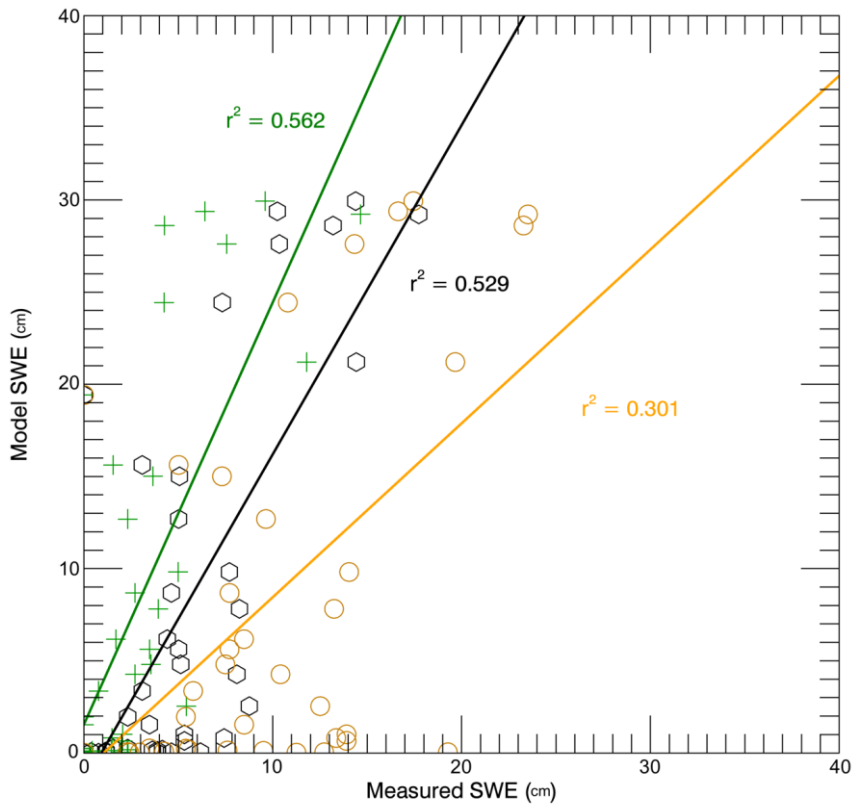


515

516 **Figure 2.** SnowModel hourly (solid lines), ERA-I daily (hashed lines) snow water equivalent (swe) accumulation and AMSR-E daily snow depth (crosses)  
517 converted to swe for fastening areas 1 (blue), 2 (green) and 3 (orange). The mean *in situ* swe and standard deviations for each area are displayed as circles at  
518 the end of November and colour coded to their respective fastening areas.

519

520



521

522 **Figure 3.** Mean (black), maximum (green) and minimum (orange) *in situ* measured snow water  
 523 equivalent (swe) for each site against mean SnowModel swe at each coincident model cell for the *in*  
 524 *situ* measurement period.

525

526

527

528

529

530

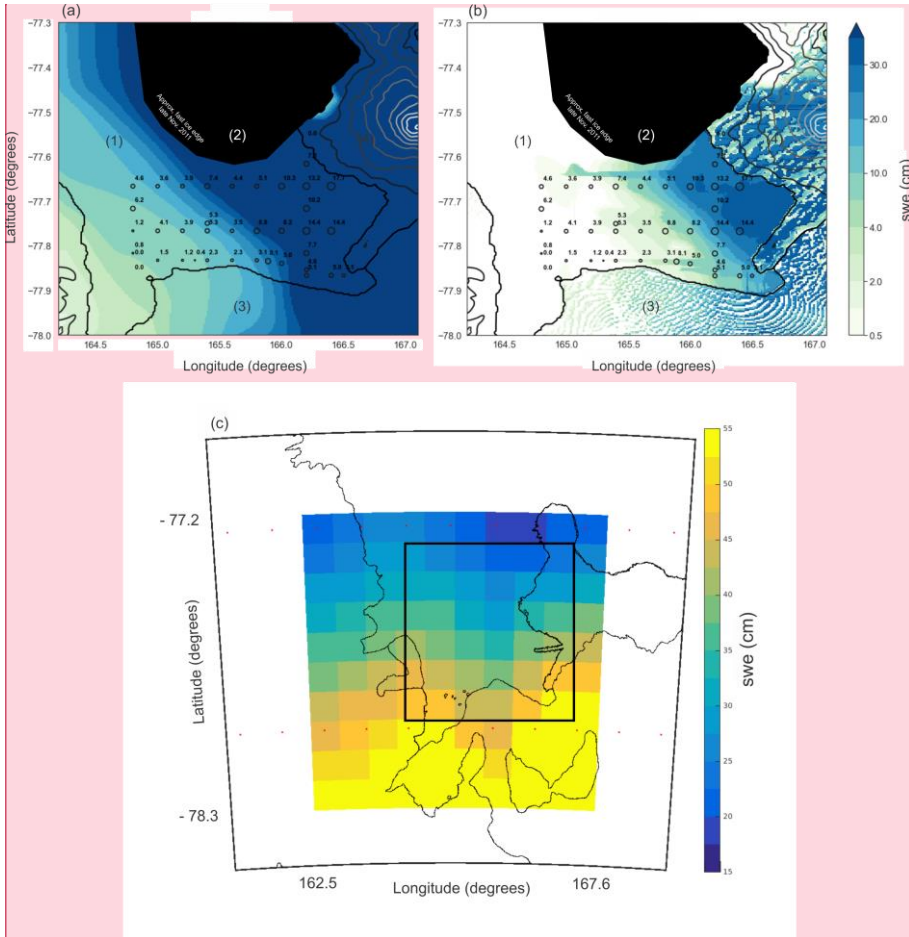
531

532

533

534





535  
 536 **Figure 4.** (a) MicroMet swe distribution (b) SnowModel swe distribution in McMurdo Sound, (1) fast  
 537 ice, (2) open water/pack ice, (3) McMurdo Ice Shelf, (4) Ross Island. The model swe distribution is the  
 538 mean of the simulation over the *in situ* measurement period (25th November-1<sup>st</sup> December). The *in situ*  
 539 measurements were converted to swe via the density measured at each site, if no measurement was  
 540 taken (21 sites) the average *in situ* snow density was used ( $385 \text{ kg m}^{-3}$ ). *In situ* measurement locations  
 541 are shown as black circles and are the mean of the 60 snow measurements taken at each site. The circle  
 542 sizes are weighted for swe to allow visualisation of the decreasing swe distribution from east to west.  
 543 Elevation contours are spaced at 400 m intervals; Mt Erebus (3,794 m) is the dominant topographic  
 544 feature on Ross Island to the east of the fast ice. (c) The interpolated 10 x 10 ERA-I grid with 1<sup>st</sup>  
 545 December accumulation total, the boundary of the SnowModel inset from (a) is shown as the black box.  
 546 The ERA-I centre points of the original grid are displayed as red dots.

**Commented [DP2]:** Figure 4 with accumulation without redistribution by wind included.

547

548

549

550 **5 Sea ice thickness**

551 In this section, we review the usefulness of the snow products by using them as inputs to  
552 equations 1-3 and infer sea ice thickness in McMurdo Sound through the growth season. Snow  
553 information, coincident in space and time for each CS-2 measurement is retrieved from the  
554 SnowModel and AMSR-E products as snow depth, while ERA-I swe is converted to snow  
555 depth using the mean *in situ* measured density.

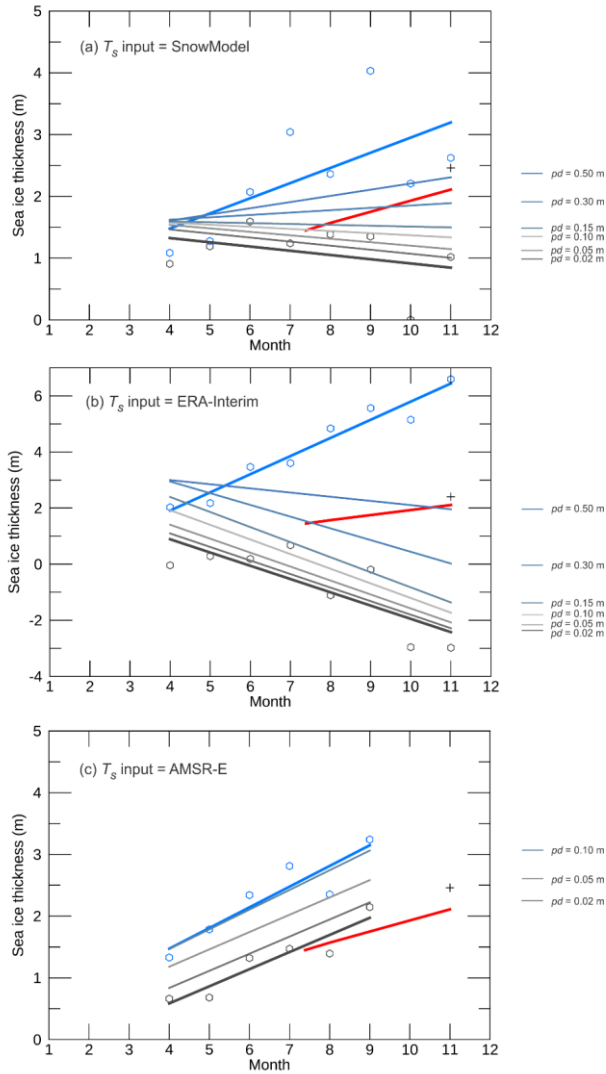
556 Sea ice thickness inferred from altimetry in McMurdo Sound will be influenced by the buoyant  
557 sub-ice platelet layer (Price et al., 2014). The *Fb* measurement used to infer thickness is  
558 representative of the solid sea ice and the layer of sub-ice platelets attached below. Therefore,  
559 comparisons to *in situ* thickness referenced in this work actually refer to the ‘mass-equivalent  
560 thickness’, that is, the resultant thickness taking account of both the solid sea ice and the sub-  
561 ice platelet layer (sub-ice platelet layer multiplied by the solid fraction). The only exception to  
562 this is the red line in Fig. 5 which is a linear fit between two measurements of consolidated sea  
563 ice thickness in July and November 2011 used here to show the sea ice thickness growth rate  
564 for comparison to CS-2 thickness trends.

565 From equations 1-3, sea ice thickness is highly sensitive to the snow-ice ratio for the measured  
566 freeboard. This results in a large range in sea ice thickness for all snow products through the  
567 growth season (Fig. 5). This range in inferred thickness is driven by the amount of snow  
568 produced by the models as Eq. 1 and Eq. 2 subtract and add the product of this value in their  
569 second terms respectively. As the snow depth increases, in some cases to higher values than  
570 the measured freeboard the *Pd* simply provides a correcting factor for this discrepancy. The  
571 AMSR-E derived thickness trend is not comparable to the model output trends as the last two  
572 months are missing. However, it is useful to highlight the importance of the snow-ice freeboard  
573 ratio. AMSR-E snow depths remain relatively stable for the duration of the study. Because of  
574 this, the ratio of ice to snow above the waterline remains very similar. In the case of the models,  
575 snow depths gradually increase and snow makes up an ever increasing proportion of mass  
576 above the waterline. If the air-snow interface (Eq. 1) is taken to represent *Fb* then the trend in  
577 sea ice thickness through the growth season is negative for SnowModel and ERA-I derived  
578 thicknesses and if the snow-ice interface (Eq. 2) is assumed the trend is too positive. The trends  
579 are more extreme for the ERA-I estimates simply because the snow loading is greater. The  
580 range in uncertainty between Eq. 1 and Eq. 2 derived thickness as means of available data for  
581 the entire growth season are 1.08 m, 4.94 m and 1.03 m for SnowModel, ERA-I and AMSR-E  
582 respectively. The mean CS-2 derived thickness values for November using Eq.1 and Eq. 2 are  
583 1.02 m (-2.98 m) for SnowModel (ERA-I) and 2.62 m (6.59 m) for SnowModel (ERA-I)  
584 respectively compared to an *in situ* thickness of 2.4 m. The trends that result in a November  
585 thickness supported by the *in situ* measurements are those that assume penetration into the  
586 snow cover, analogous with the retracked surface representing a surface between the air-snow  
587 and snow ice interfaces. For thicknesses derived using the models to match *in situ* thickness  
588 large *Pd* values of 0.5 m are required given the higher snow depth values. These values are  
589 lower for AMSR-E as the snow loading is less.

590 The differences in the snow depths from each model result make it difficult to constrain what  
591 *Pd* value provides CS-2 thicknesses that agree best with measured thickness. To assess the  
592 penetration uncertainty further we use interpolated *in situ* measurements for snow depth as  
593 input to the sea ice thickness calculation. We reduce the CS-2 measurements used in this

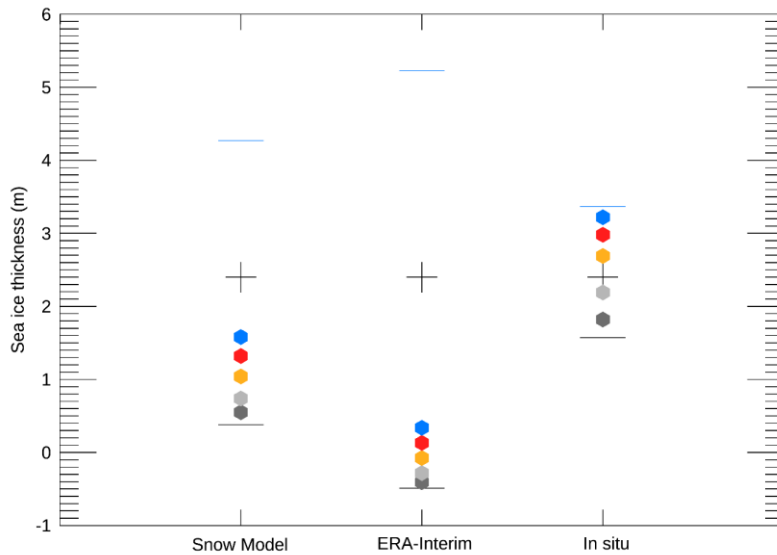
594 comparison to the same area bounded by *in situ* measurements. The total range in estimated  
595 sea ice thickness using interpolated *in situ* snow depth between equations 1 and 2 is 1.7 m. For  
596  $Pd$  values 0.02 m through 0.20 m the best agreement between *in situ* thickness and CS-2 derived  
597 thickness is found between 0.05 and 0.10 m (Fig. 6 – third column, ‘In situ’). The CS-2  
598 thickness is only 0.02 m thicker than *in situ* thickness for this particular dataset when  $Pd = 0.07$   
599 m. The range in SnowModel derived thickness between Eqs. 1 and 2 is nearly 4 m while the  
600 range when using the ERA-I data set is very large at 5.7 m (Fig. 6). Again this large range in  
601 thickness reflects the higher average snow depth produced by ERA-I. The deeper snow creates  
602 a larger range of snow-to-ice ratios for freeboard.

603



604

605 **Figure 5.** Sea ice thickness trends derived by CS-2 freeboard measurements with snow data provided  
 606 by (a) SnowModel, (b) ERA-I and (c) AMSR-E. Grey dots and bold linear fit are sea ice thickness  
 607 calculated using equation 1, blue dots and bold linear fit using equation 2 and thin lines between them  
 608 equation 3 with varying penetration factors ( $Pd$ ). The red line shows sea ice thickness from *in situ*  
 609 measurements of consolidated sea ice thickness with a tape measure taken in July and November in one  
 610 location in the south of McMurdo Sound joined assuming a constant growth rate. The black plus sign  
 611 is the mean 'mass-equivalent thickness' from all *in situ* measurements in November. This is slightly  
 612 thicker than the end of season thickness indicated by the red line given it takes account of the influence  
 613 of the sub-ice platelet layer. This black plus sign is what CS-2 thickness should be compared to (see  
 614 text).



615  
 616 **Figure 6.** The range in CS-2 derived sea ice thickness in November using snow inputs from SnowModel  
 617 and ERA-I compared to snow input from *in situ* interpolated snow depths. Thickness derived from  
 618 equations 1 and 2 are shown with the grey and blue lines respectively and for equation 3 the dots are  
 619 colour coded for different penetration depths (*Pd*); dark grey = 0.02 m, light grey = 0.05 m, orange =  
 620 0.10 m, red = 0.15 m and blue = 0.20 m. Black plus signs show *in situ* 'mass-equivalent thickness'. This  
 621 comparison is produced from all CS-2 data height retrievals available over the *in situ* measurement area  
 622 in November ( $n = 279$ ).

## 623 6 Discussion

624 In this section, the performance of the snow depth retrieval methods and CS-2 thickness  
 625 uncertainty is evaluated. We briefly discuss their future applicability to larger Antarctic sea ice  
 626 areas.

627 Any method attempting to accumulate snow on sea ice requires the establishment of a starting  
 628 date from which a sea ice surface is present. This approach used Envisat ASAR imagery and  
 629 motion between scenes to identify when the sea ice fastened. Freezing may have started prior  
 630 to the fastening date but the authors are unaware of any other method to monitor sea ice  
 631 formation at the required spatial resolution for SnowModel. Sea ice could have begun to form  
 632 slightly before this date, which, assuming a net gain in snow would result in an improvement  
 633 in SnowModel's performance in area 1, but increased separation between *in situ* validation and  
 634 SnowModel in areas 2 and 3. ERA-I performance would be worse in all cases, AMSR-E would  
 635 not be impacted as it is a real-time snow depth measurement. In larger open water areas,  
 636 passive microwave sea ice concentration information could be used to establish the formation  
 637 date. Detail would be lost via this method given the high (200 m) resolution of SnowModel  
 638 against the coarser resolution passive microwave data. Early snow fall on more dynamic pack  
 639 ice will also be subject to flooding, sea spray (both likely to result in snow-ice formation) and  
 640 loss to leads. These uncertainties must all be considered in future work.

641 Modelled snow depths have been evaluated in previous work over Antarctic sea ice (Maksym  
642 and Markus, 2008), but the study produced precipitation data while this assessment takes the  
643 next step by using a model that accounts for surface transportation, a significant redistribution  
644 mechanism in the Antarctic. Without this model component included the precipitation provided  
645 by MicroMet (downscaled PWRP) provides very poor estimates of snow depth on sea. Leonard  
646 and Maksym (2011) report that over half of precipitation over the Southern Ocean could be  
647 lost to leads and the application of any model to construct snow depth on sea ice in open sea  
648 areas will need to account for this. In coastal regions, local topography will also play a key  
649 role, such is the case in McMurdo Sound where Ross Island acts to encourage snow  
650 accumulation on the eastern portion of the sea ice cover. This was well replicated in  
651 SnowModel although the overestimation of snow was driven by unrealistic values in this area,  
652 the model likely accumulating too much snow due to this topographic barrier. Smaller scale  
653 snow features such as snow drifts and snow dunes should also be accounted for in future work,  
654 as applied in a recent study by Liston et al. (2018). These meter-scale features will be important  
655 to capture, especially to support compatibility with smaller satellite altimeter footprints, in  
656 particularly ICESat-2 (Markus et al., 2017). This work used fast ice to reduce the uncertainty  
657 associated with pack ice and used available *in situ* data to validate the snow products. To build  
658 on this approach, and make its application valuable in the Southern Ocean, sea ice motion  
659 within the SnowModel domain must be incorporated.

660 We find the ERA-I mean swe to be 20 cm higher than mean *in situ* swe in McMurdo Sound.  
661 In area 1 ERA-I swe is an order of magnitude higher than *in situ* swe, while in areas 2 and 3 it  
662 is over double the value. These create very high, unrealistic snow depths which causes a large  
663 range in CS-2 derived thickness using Eqs. 1-3. This is a very poor result and the product is  
664 inadequate to infer sea ice thickness when combined with altimetry data. Of further interest is  
665 that the clear longitudinal gradient in snow depth as indicated by SnowModel and measured *in*  
666 *situ* (November only) is not produced by ERA-I, swe values are lower in the central fast ice  
667 area and higher in the western and eastern areas. The performance of ECMWF reanalysis  
668 products over the satellite period has been reported as good when compared to Antarctic coastal  
669 stations (Bromwich and Fogt, 2004), but there is limited data available to assess the accuracy  
670 of these data over Antarctic sea ice. ERA-I ranked best among five assessed models for its  
671 depiction of interannual variability and overall change in precipitation, evaporation and total  
672 precipitable water over the Southern Ocean (Nicolas and Bromwich, 2011). Maksym & Markus  
673 (2008) used ERA-40 reanalysis for a snow assessment of the Antarctic sea ice pack but had  
674 difficulties in evaluating its accuracy. A first step to improve reanalysis results will be to  
675 incorporate snow redistribution (including snow loss to leads) and parameterisations for this  
676 could be built from wind vectors provided by the same reanalysis data.

677 In general, when compared to SnowModel, AMSR-E underestimates snow depth in areas 2 and  
678 3 (eastern Sound) and overestimates snow depth in area 1 (western Sound). The snow  
679 distribution gradient from east to west is reversed in the AMSR-E dataset. Worby et al. (2008b)  
680 report that AMSR-E snow depths were significantly lower than *in situ* measurements on sea  
681 ice in the East Antarctic and that sea ice roughness is a major source of error using passive  
682 microwave retrieval techniques. However, they also conclude that when compared to basin-  
683 wide observations from ASPECT large differences of up to + 20 cm in the Weddell Sea and +  
684 5-10 cm in the Ross Sea were noted in the AMSR-E snow depths. Vessels are restricted in their  
685 ability to sample in heavily deformed and thicker sea ice areas where the snow is typically

**Commented [DP3]:** New sentence referencing poor performance of PWRP precipitation without inclusion of redistribution by wind.

686 higher. Because of this, it is postulated that shipborne observations of *in situ* snow thickness  
687 were biased low in comparison to AMSR-E snow depth. More work is required to validate  
688 passive microwave snow depth estimates over Antarctic sea ice. No detailed sea ice surface  
689 condition survey was completed for this investigation, however from visual observations sea  
690 ice had clearly been subjected to dynamics in the west, whereas ice was very level in the east.  
691 It is possible that snow depth was underrepresented here by *in situ* measurements and that  
692 rougher sea ice in the west affected the AMSR-E retrieval algorithm. Because of the failure of  
693 the instrument, we are unable to compare AMSR-E snow depth directly to *in situ*  
694 measurements.

Commented [DP4]: Sentence about ASPECT revised

695 CS-2 has difficulty estimating freeboard over thin ice areas (Price et al., 2015, Ricker et al.,  
696 2014, Wingham et al., 2006). Here, at the beginning of the growth season CS-2 generally  
697 overestimates sea ice thickness with mean April values inferred using snow data from  
698 SnowModel and ERA-I of around 1 m (with the exception of AMSR-E assuming the air-snow  
699 interface is measured  $T_i = 0.66$  m). Other investigations indicate that sea ice thickness in  
700 McMurdo Sound in April is between 0.5-0.8 m (Frazer et al., 2018, Gough et al., 2012, Purdie  
701 et al., 2006) . This represents a large obstacle to overcome for the application of CS-2 in the  
702 Southern Ocean as the mean thickness of Antarctic sea ice is only 0.87 m as reported from  
703 ship-based observations (Worby et al., 2008a). This supports the need for multisensor analysis,  
704 perhaps using methods already employed in the Arctic (Ricker et al., 2017, Kaleschke et al.,  
705 2012, Kwok et al., 1995). As discussed in section 2.4 assumptions must be made about what  
706 surface the freeboard measurement represents. In general, using the two modelled snow  
707 products (because trends from AMSR-E are incomplete), the thicknesses derived assuming the  
708 air-snow interface is freeboard are too thin and those assuming the snow-ice interface is  
709 freeboard are too thick, a simple consequence of the density dependent hydrostatic equilibrium  
710 assumption. By using the interpolated *in situ* measured snow depth as the snow thickness input  
711 to the thickness calculation, the error is minimised. With this, we find CS-2 thickness to  
712 correlate best with *in situ* thickness if  $Pd$  values are between 0.05-0.10 m. This is supported by  
713 other work in the study area (Price et al., 2015) who estimated the ESA elevation to be between  
714 the air-snow and snow-ice interfaces when sea surface height error was ruled out via a manual  
715 sea surface classification. Also recent work in the Arctic suggests that the height that represents  
716 radar freeboard provided by the ESA Level 2 product is closer to the air-snow interface than  
717 the snow-ice interface (King et al., 2018).

718 Having confidence in the results assumes that the sea surface height has been accurately  
719 identified for each CS-2 track. Freeboard errors from automated sea surface height  
720 identification were in the order of 0.05 m when compared to supervised procedures in the study  
721 area (Price et al., 2015). To eliminate this uncertainty throughout the study period the sea  
722 surface would need to be manually identified for each individual CS-2 track. This is not  
723 practical for basin-scale assessments and confidence needs to be built in the sea surface height  
724 identification algorithm. The modification of the sea surface height will apply a systematic  
725 increase or decrease in freeboard making each thickness from each assumption thicker or  
726 thinner. The freeboard measurements exhibit an unexpected decrease in October and  
727 November and it is impossible to discern whether this is forced by a sea surface height that is  
728 too high, or a change in the sea ice surface conditions that causes a decrease in the freeboard  
729 measurement, an additional uncertainty. More detailed *in situ* investigations, with surface  
730 roughness and snow characteristic statistics at the scale of the altimeter footprint are required

731 before a seasonally varying  $Pd$  can be applied with any confidence. As this analysis was  
732 focused on the combination of independent snow products and CS-2 altimeter data, the range  
733 in sea ice density has not been taken into account. We have confidence in the middle ground  $\rho_i$   
734 value used from previous work in McMurdo Sound (Price et al., 2014) but this is another source  
735 of uncertainty for regional and basin-scale assessments.

## 736 7 Conclusions

737 This work has evaluated the ability of three independent techniques to provide snow depth on  
738 fast ice in the coastal Antarctic. SnowModel accurately captures the *in situ* measured snow  
739 distribution in November 2011 and produces a swe mean value that is 0.02 m above the mean  
740 of *in situ* validation, but when sea ice is segmented by fastening date large deviations of up to  
741 5 cm are present in the east where the model has overestimated snow depth. This accurately  
742 captures the mechanism of snowfall and transport driven by the topography of Ross Island, but  
743 the rates are higher than in reality. ERA-I swe is 20 cm higher than *in situ* measurements and  
744 the gradient of the snow distribution produced by the analysis does not match that measured *in*  
745 *situ*. A positive bias in accumulation should be expected from ERA-I as no snow redistribution  
746 mechanism is included. Any future work making use of precipitation reanalysis over Antarctic  
747 sea ice must include snow redistribution by wind, shown here by SnowModel to improve  
748 results. AMSR-E snow depth information suffers from problems already documented in the  
749 literature, and we find that its performance may have again been influenced by rough sea ice.  
750 The snow distribution produced by AMSR-E was opposite to that provided by SnowModel and  
751 measured *in situ* at the end of the growth season. We were unable to validate the instrument  
752 due to its failure two months before the *in situ* data was collected. The uncertainty in the snow  
753 depth estimates manifest themselves in the sea ice thickness estimates from CS-2. The range  
754 in sea ice thickness uncertainty from the assumption that the snow surface or ice surface  
755 represents freeboard, as means of the entire growth season are 1.08 m, 4.94 m and 1.03 m for  
756 SnowModel, ERA-Interim and AMSR-E respectively. Using interpolated *in situ* snow  
757 information, we find CS-2 freeboard measurements provided by the ESA retracker agree best  
758 with *in situ* measured thickness if a dominant scattering horizon 0.07 m beneath the air-snow  
759 interface is assumed, in agreement with recent literature. It is impossible to **confidently**  
760 constrain this number without reducing uncertainty in the established sea surface height from  
761 which the freeboard is estimated. This work demonstrates the need to reduce the uncertainty  
762 associated with the ambiguity of the altimeter radar freeboard measurement over Antarctic sea  
763 ice. Sea ice in McMurdo Sound is atypical of Antarctic pack ice, so improved understanding  
764 of the CS-2 freeboard measurement over varying snow and sea ice conditions in open water  
765 areas will be critical to accurately provide sea ice thickness estimates for the Southern Ocean.

766 Here, we show that modelled snow information has the potential to produce a time series of  
767 snow depth on Antarctic sea ice. However, major developments in modelling capability are  
768 required before their snow products can provide useful information for use in combination with  
769 altimetry data to provide Antarctic sea ice thickness. With improvements to redistribution  
770 mechanisms and adequate representation of the effect of topographic features, atmospheric  
771 models could be used as an alternative to contemporary passive microwave algorithms. Future  
772 work should begin to assess the usefulness of SnowModel products over the larger pack ice  
773 areas, and critically develop a method to (1) incorporate sea ice drift through the atmospheric  
774 model domains, and (2) account for snow loss to leads. If these two influences can be  
775 adequately incorporated, SnowModel could provide a valuable resource for snow and sea ice

Commented [DP5]: Amended to 'confidently'



776 thickness investigations over the wider Antarctic sea ice area, especially where snow depth is  
777 high and passive microwave techniques are non-informative.

## 778 **8 Acknowledgments**

779 Gratitude is shown for the support of Antarctica New Zealand and Scott Base staff during the  
780 2011/12 Antarctic field season permitting the collection of *in situ* snow and sea ice  
781 measurements, and the members of field team K053. We thank Glen E. Liston for providing  
782 the code for SnowModel. Further thanks is given to Oliver Marsh and Christian Wild for  
783 productive discussions about the topic. This work was partially supported by NIWA  
784 subcontract C01X1226 (Ross Sea Climate and Ecosystem) and the Marsden Fund Council from  
785 Government funding, managed by Royal Society Te Apārangi. We are grateful to Victoria  
786 Landgraf, Troy Beaumont, and Grant Cottle from Antarctica New Zealand's Scott Base 2011  
787 winter-over team for making the July sea ice thickness measurements as part of the winter  
788 support of a University of Otago Research Grant funded project (PI: Pat Langhorne, AI: Inga  
789 Smith). We thank Peter Green and Inga Smith for their insights into the 2011 sea ice growth  
790 rates, which were supported by the fieldwork and analytical efforts of Greg Leonard, Alex  
791 Gough, Tim Haskell, Pat Langhorne, Jonothan Everts, and by the technical advice of Joe  
792 Trodahl and Daniel Pringle, and the technical support of Myles Thayer, Peter Stroud and  
793 Richard Sparrow. A final thanks is given to Eamon Frazer and Pat Langhorne for the time given  
794 to discussions about and analysis of seawater density in the study region. This research was  
795 completed at Gateway Antarctica, University of Canterbury, Christchurch, New Zealand.

## 796 **9 References**

- 797 Agustsson, H., and Olafsson, H.: Simulating a severe windstorm in complex terrain. *Meteorol*  
798 *Atmos Phys.*, 103, 173–185, doi: 10.1007/s00703-008-0347-y, 2007.
- 799 Armitage, T. W. K., and Davidson, M. W. J.: Using the Interferometric Capabilities of the ESA  
800 CryoSat-2 Mission to Improve the Accuracy of Sea Ice Freeboard Retrievals, in *IEEE*  
801 *Transactions on Geoscience and Remote Sensing.*, vol. 52, no. 1, pp. 529-536, doi:  
802 10.1109/TGRS.2013.2242082, 2014.
- 803  
804 Beaven, S. G., Lockhart, G. L., Gogineni, S. P., Hossetnmostafa, A. R., Jezek, K., Gow, A. J.,  
805 Perovich, D. K., Fung, A. K., and Tjuatja, S.: Laboratory measurements of radar backscatter  
806 from bare and snow-covered saline ice sheets. *International Journal of Remote Sensing*, 16,  
807 851-876, 1995.
- 808 Bouffard, J.: CryoSat-2 Level 2 product evolutions and quality improvements in Baseline C.  
809 Available at: [https://earth.esa.int/documents/10174/1773005/C2-Evolution-BaselineC-](https://earth.esa.int/documents/10174/1773005/C2-Evolution-BaselineC-Level2-V3)  
810 [Level2-V3](https://earth.esa.int/documents/10174/1773005/C2-Evolution-BaselineC-Level2-V3). 2015
- 811 Bromwich, D.H., Hines K.M., and Bai, L.S.: Development and testing of Polar WRF: 2. Arctic  
812 Ocean, *J. Geophys. Res.*, 114, D08122, doi: 10.1029/2008JD010300, 2009.
- 813 Bromwich, D. H., and Fogt, R. L.: Strong Trends in the Skill of the ERA-40 and NCEP–NCAR  
814 Reanalyses in the High and Midlatitudes of the Southern Hemisphere, 1958–2001, *Journal of*  
815 *Climate.*, 17, 4603-4619, doi: 10.1175/3241.1, 2004.
- 816 Chen, F., and Dudhia, J.: Coupling an Advanced Land Surface–Hydrology Model with the  
817 Penn State–NCAR MM5 Modeling System. Part I: Model Implementation and Sensitivity,

818 Monthly Weather Review., 129, 569-585, doi: 10.1175/1520-  
819 0493(2001)129<0569:CAALSH>2.0.CO;2, 2001.

820 Comiso, C., Cavalieri, J. & Markus, T.: Sea Ice Concentration, Ice Temperature, and Snow  
821 Depth Using AMSR-E Data, IEEE Transactions on Geoscience and Remote Sensing., 41, 243-  
822 252, doi: 10.1109/TGRS.2002.808317, 2003.

823 Dee, D. P., Uppala, S. M., Simmons, A. J., Berrisford, P., Poli, P., Kobayashi, S., Andrae, U.,  
824 Balmaseda, M. A., Balsamo, G., Bauer, P., Bechtold, P., Beljaars, A. C. M., van de Berg, L.,  
825 Bidlot, J., Bormann, N., Delsol, C., Dragani, R., Fuentes, M., Geer, A. J., Haimberger, L.,  
826 Healy, S. B., Hersbach, H., Hólm, E. V., Isaksen, I., Kållberg, P., Köhler, M., Matricardi, M.,  
827 McNally, A. P., Monge-Sanz, B. M., Morcrette, J. J., Park, B. K., Peubey, C., De Rosnay, P.,  
828 Tavolato, C., Thépaut, J. N., and Vitart, F.: The ERA-I reanalysis: configuration and  
829 performance of the data assimilation system, Quarterly Journal of the Royal Meteorological  
830 Society., 137, 553-597, doi: 10.1002/qj.828, 2011.

831 Drinkwater, M.: Ku-band airborne radar altimeter observations of marginal sea ice during the  
832 1984 Marginal Ice Zone Experiment, J. Geophys. Res., 96(C3), 4555-4572, doi:  
833 doi.org/10.1029/90JC01954, 1991.

834 Dudhia, J.: Numerical study of convection observed during the winter monsoon experiment  
835 using a mesoscale two-dimensional model, Journal of Atmospheric Sciences., 46, 3077-3107,  
836 doi: 10.1175/1520-0469(1989)046<3077:NSOCOD>2.0.CO;2, 1989.

837 Fichefet, T., and Maqueda, M. A. M.: Modelling the influence of snow accumulation and snow-  
838 ice formation on the seasonal cycle of the Antarctic sea-ice cover, Climate Dynamics., 15, 251-  
839 268, doi: 10.1007/s003820050280, 1999.

840 Frazer, E. K., Langhorne, P. J., Williams, M. J. M., Goetz, K. T., and Costa, D. P.: A method  
841 for correcting seal-borne oceanographic data and application to the estimation of regional sea  
842 ice thickness, Journal of Marine Systems., doi: 10.1016/j.jmarsys.2018.08.002, 2018.

843 Giles, K. A., Laxon, S. W., and Worby, A. P.: Antarctic sea ice elevation from satellite radar  
844 altimetry, Geophysical Research Letters., 35, L03503, doi: 10.1029/2007GL031572, 2008.

845 Gough, A. J., Mahoney, A. R., Langhorne, P. J., Williams, M. J. M., and Haskell, T. G.: Sea  
846 ice salinity and structure: A winter time series of salinity and its distribution, Journal of  
847 Geophysical Research: Oceans., 117, C03008, doi:10.1029/2011JC007527, 2012.

848 Hallikainen, M., Ulaby, F., and Abdelrazik, M.: Dielectric properties of snow in the 3 to 37  
849 GHz range, IEEE Transactions on Antennas and Propagation., 34, 1329-1340, 1986.

850 Hendricks, S., Stenseng, L., Helm, V., and Haas, C.: Effects of surface roughness on sea ice  
851 freeboard retrieval with an Airborne Ku-Band SAR radar altimeter, In International  
852 Geoscience and Remote Sensing Symposium (IGARSS 2010), 25-30 July 2010, Proceedings.  
853 Institute of Electrical and Electronics Engineers, Piscataway, NJ, 3126-3129, doi:  
854 10.1109/IGARSS.2010.5654350, 2010.

855 Hines, K. M., Bromwich, D. H., Bai, L., Bitz, C. M., Powers, J. G., and Manning, K. W. Sea  
856 Ice Enhancements to Polar WRF, Monthly Weather Review., 143, 2363-2385, doi:  
857 10.1175/MWR-D-14-00344.1, 2015.

858 Hong, S.-Y., and Lim, J.-O. J.: The WRF Single-Moment 6-Class Microphysics Scheme  
859 (WSM6), *Journal of the Korean Meteorological Society.*, 42, 129-151, 2006.

860 Kaleschke, L., Tian-kunze, X., Maaß, N., Mäkynen, M., and Drusch, M.: Sea ice thickness  
861 retrieval from SMOS brightness temperatures during the Arctic freeze-up period, *Geophysical  
862 Research Letters.*, 39, L05501, doi: 10.1029/2012GL050916, 2012.

863 Kern, S., and Ozsoy-Çiçek, B.: Satellite Remote Sensing of Snow Depth on Antarctic Sea Ice:  
864 An Inter-Comparison of Two Empirical Approaches, *Remote Sensing.*, 8(6), 450, doi:  
865 10.3390/rs8060450, 2016.

866 Kern, S., Ozsoy-Çiçek, B., Willmes, S., Nicolaus, M., Haas, C. & Ackley, S.: An  
867 intercomparison between AMSR-E snow-depth and satellite C- and Ku-band radar backscatter  
868 data for Antarctic sea ice, *Annals of Glaciology.*, 52(57), 279-290.  
869 doi:10.3189/172756411795931750, 2011.

870 King, J., Skourup, H., Hvidegaard, S. M., Rosel, A., Gerland, S., Spreen, G., Polashenski, C.,  
871 Helm, V., and Liston, G. E.: Comparison of freeboard retrieval and ice thickness calculation  
872 from ALS, ASIRAS, and CryoSat-2 in the Norwegian Arctic to field measurements made  
873 during the N-ICE2015 expedition, *Journal of Geophysical Research: Oceans.*, 123, 1123–1141,  
874 doi: 10.1002/ 2017JC013233, 2018.

875  
876 Kurtz, N. T., Galin, N., and Studinger, M.: An improved CryoSat-2 sea ice freeboard retrieval  
877 algorithm through the use of waveform fitting, *The Cryosphere.*, 8, 1217-1237,  
878 <https://doi.org/10.5194/tc-8-1217-2014>, 2014.

879 Kurtz, N. T., and Markus, T.: Satellite observations of Antarctic sea ice thickness and volume,  
880 *Journal of Geophysical Research: Oceans.*, 117, C08025, doi: 10.1029/2012JC008141, 2012.

881 Kwok, R.: Simulated effects of a snow layer on retrieval of CryoSat-2 sea ice freeboard,  
882 *Geophysical Research Letters.*, 41, 5014–5020, doi: 10.1002/2014GL060993, 2014.

883 Kwok, R., and Cunningham, G. F.: ICESat over Arctic sea ice: Estimation of snow depth and  
884 ice thickness, *Journal of Geophysical Research: Oceans.*, 113, C08010,  
885 doi: 10.1029/2008JC004753, 2008.

886 Kwok, R., Nghiem, S. V., Yueh, S. H., and Huynh, D. D.: Retrieval of thin ice thickness from  
887 multifrequency polarimetric SAR data, *Remote Sensing of Environment.*, 51, 361-374, doi:  
888 10.1016/0034-4257(94)00017-H, 1995.

889 Laxon, S., Peacock, N. & Smith, D.: High interannual variability of sea ice thickness in the  
890 Arctic region, *Nature.*, 425, 947-950, doi: 10.1038/nature02050, 2003.

891 Laxon, S. W., Giles, K. A., Ridout, A. L., Wingham, D. J., Willatt, R., Cullen, R., Kwok, R.,  
892 Schweiger, A., Zhang, J., Haas, C., Hendricks, S., Krishfield, R., Kurtz, N., Farrell, S., and  
893 Davidson, M.: CryoSat-2 estimates of Arctic sea ice thickness and volume, *Geophysical  
894 Research Letters.*, 40, 732-737, doi: 10.1002/grl.50193, 2013.

895• Leonard, K. C., and Maksym, T.: The importance of wind-blown snow redistribution to snow  
896 accumulation on Bellingshausen Sea ice, *Annals of Glaciology.*, 52, 271-278, doi:  
897 10.3189/172756411795931651, 2011.

898

899 Liston, G. E., Polashenski, C., Rösel, A., Itkin, P., King, J., Merkouriadi, I., and Haapala, J.:  
900 A Distributed Snow Evolution Model for Sea Ice Applications (SnowModel), *J. Geophys. Res.*  
901 *Oceans.*, Accepted Author Manuscript, doi:10.1002/2017JC013706, 2018.

902 Liston, G. E., and Hiemstra, C. A.: Representing Grass- and Shrub-Snow-Atmosphere  
903 Interactions in Climate System Models, *Journal of Climate.*, 24, 2061-2079, doi:  
904 10.1175/2010JCLI4028.1, 2011.

905 Liston, G. E., and Hiemstra, C. A.: A Simple Data Assimilation System for Complex Snow  
906 Distributions (SnowAssim), *Journal of Hydrometeorology.*, 9, 989-1004, doi:  
907 10.1175/2008JHM871.1, 2008.

908• Liston, G. E., Haehnel, R. B., Sturm, M., Hiemstra, C. A., Berezovskaya, S., and Tabler, R. D.  
909 Instruments and Methods Simulating complex snow distributions in windy environments using  
910 SnowTran-3D, *Journal of Glaciology.*, 53, 241-256, doi: 10.3189/172756507782202865, 2007.  
911

912 Liston, G. E., and Elder, K.: A Distributed Snow-Evolution Modeling System (SnowModel),  
913 *Journal of Hydrometeorology.*, 7, 1259-1276, doi: 10.1175/JHM548.1, 2006a.

914 Liston, G. E., and Elder, K.: A Meteorological Distribution System for High-Resolution  
915 Terrestrial Modeling (MicroMet), *Journal of Hydrometeorology.*, 7, 217-234, doi:  
916 10.1175/JHM486.1, 2006b.

917 Liston, G. E., and Winther, J.-G.: Antarctic Surface and Subsurface Snow and Ice Melt Fluxes,  
918 *Journal of Climate.*, 18, 1469-1481, doi: 10.1175/JCLI3344.1, 2005.

919 Liston, G. E., Pielke, R. A., and Greene, E. M.: Improving first-order snow-related deficiencies  
920 in a regional climate model, *Journal of Geophysical Research: Atmospheres.*, 104, 19559-  
921 19567, doi: 10.1029/1999JD900055, 1999.

922• Liston, G. E. & Sturm, M.: A snow-transport model for complex terrain, *Journal of Glaciology.*,  
923 44, 498-516, doi: 10.3189/S0022143000002021, 1998.  
924•

925 Maksym, T., and Markus, T.: Antarctic sea ice thickness and snow-to-ice conversion from  
926 atmospheric reanalysis and passive microwave snow depth, *Journal of Geophysical Research:*  
927 *Oceans.*, 113, C02S12, doi:10.1029/2006JC004085, 2008.

928 Markus, T., Neumann, T., Martino, A., Abdalati, W., Brunt, K., Csatho, B., Farrell, S., Fricker,  
929 H., Gardner, A., Harding, D., Jasinski, M., Kwok, R., Magruder, L., Lubin, D., Luthcke, S.,  
930 Morison, J., Nelson, R., Neuenschwander, A., Palm, S., Popescu, S., Shum, C.K., Schutz, B.E.  
931 Smith, B., Yang, Y., and Zwally, J.: The Ice, Cloud, and land Elevation Satellite-2 (ICESat-2):  
932 Science requirements, concept, and implementation, *Remote Sensing of Environment.*, 190,  
933 260-273, doi: 10.1016/j.rse.2016.12.029, 2017.

934 Markus, T., and Cavalieri, D. J.: Snow Depth Distribution Over Sea Ice in the Southern Ocean  
935 from Satellite Passive Microwave Data. *Antarctic Sea Ice: Physical Processes, Interactions and*  
936 *Variability*, American Geophysical Union, M. O. Jeffries (Ed.), doi:10.1029/AR074p0019,  
937 1998.

938• Markus, T., and Cavalieri, D. J.: Interannual and regional variability of Southern Ocean snow  
939 on sea ice, *Annals of Glaciology.*, 44, 53-57, doi: 10.3189/172756406781811475, 2006.  
940•

941 Massom, R. A., Eicken, H., Hass, C., Jeffries, M. O., Drinkwater, M. R., Sturm, M., Worby,  
942 A. P., Wu, X., Lytle, V. I., Ushio, S., Morris, K., Reid, P. A., Warren, S. G., and Allison, I.:  
943 Snow on Antarctic sea ice, *Reviews of Geophysics.*, 39(3), 413–445,  
944 doi:10.1029/2000RG000085, 2001.

945 Maykut, G., and Untersteiner, N.: Some results from a time dependent thermodynamic model  
946 of sea ice, *J. Geophys. Res.*, 76, 1550-1575, 1971.

947 Mernild, S.H., Liston, G.E., Hasholt, B., and Knudsen, N.T.: Snow distribution and melt  
948 modeling for Mittivakkat Glacier, Ammassalik Island, southeast Greenland, *J.*  
949 *Hydrometeorology.*, 7, 808-824, doi: 10.1175/JHM522.1, 2006.

950 Mlawer, E. J., Taubman, S. J., Brown, P. D., Iacono, M. J., and Clough, S. A.: Radiative transfer  
951 for inhomogeneous atmospheres: RRTM, a validated correlated-k model for the longwave,  
952 *Journal of Geophysical Research: Atmospheres.*, 102, 16663-16682, 1997.

953 Nakanishi, M.: Improvement of the Mellor-Yamada turbulence closure model based on large-  
954 eddy simulation data, *Boundary Layer Meteorology.*, 99, 349-378, doi:  
955 10.1023/A:1018915827400, 2001.

956 Nakanishi, M., and Niino, H.: An Improved Mellor–Yamada Level-3 Model with  
957 Condensation Physics: Its Design and Verification, *Boundary-Layer Meteorology.*, 112, 1-31,  
958 doi:10.1023/B:BOUN.0000020164.04146.98, 2004.

959 Nakanishi, M., and Niino, H.: An Improved Mellor–Yamada Level-3 Model: Its Numerical  
960 Stability and Application to a Regional Prediction of Advection Fog, *Boundary-Layer*  
961 *Meteorology.*, 119, 397-407, doi: 10.1007/s10546-005-9030-8, 2006.

962 Nicolas, J. P., and Bromwich, D. H.: Precipitation Changes in High Southern Latitudes from  
963 Global Reanalyses: A Cautionary Tale, *Surveys in Geophysics.*, 32, 475-494, doi:  
964 10.1007/s10712-011-9114-6, 2011.

965 Olafsson, H., and Agustsson H.: Gravity wave breaking in easterly flow over Greenland and  
966 associated low level barrier-and reverse tip-jets, *Meteorol. Atmos. Phys.*, 104, 191-197, doi:  
967 10.1007/s00703-009-0024-9, 2009.

968• Pope, A., Wagner, P., Johnson, R., Shutler, J. D., Baeseman, J., and Newman, L.: Community  
969 review of Southern Ocean satellite data needs, *Antarctic Science.*, 29, 97-138, doi:  
970 10.1017/S0954102016000390, 2016.

971•

972• Price, D., Beckers, J., Ricker, R., Kurtz, N., Rack, W., Haas, C., Helm, V., Hendricks, S.,  
973 Leonard, G., and Langhorne, P. J.: Evaluation of CryoSat-2 derived sea-ice freeboard over fast  
974 ice in McMurdo Sound, Antarctica, *Journal of Glaciology.*, 61, 285-300, doi:  
975 10.3189/2015JoG14J157, 2015.

976

977 Price, D., Rack, W., Langhorne, P. J., Haas, C., Leonard, G., and Barnsdale, K.: The sub-ice  
978 platelet layer and its influence on freeboard to thickness conversion of Antarctic sea ice, *The*  
979 *Cryosphere.*, 8, 1031-1039, doi: 10.5194/tc-8-1031-2014, 2014.

980• Purdie, C. R., Langhorne, P. J., Leonard, G. H., and Haskell, T. G.: Growth of first-year landfast  
981 Antarctic sea ice determined from winter temperature measurements, *Annals of Glaciology.*,  
982 44, 170-176, doi: 10.3189/172756406781811853, 2006.

983•  
984 Ricker, R., Hendricks, S., Helm, V., Skourup, H., and Davidson, M.: Sensitivity of CryoSat-2  
985 Arctic sea-ice freeboard and thickness on radar-waveform interpretation, *The Cryosphere.*, 8,  
986 1607-1622, doi: 10.5194/tc-8-1607-2014, 2014.

987 Ricker, R., Hendricks, S., Kaleschke, L., Tian-Kunze, X., King, J., and Haas, C.: A weekly  
988 Arctic sea-ice thickness data record from merged CryoSat-2 and SMOS satellite data, *The*  
989 *Cryosphere.*, 11, 1607-1623, doi: 10.5194/tc-11-1607-2017, 2017.

990 Schwegmann, S., Rinne, E., Ricker, R., Hendricks, S., and Helm, V.: About the consistency  
991 between Envisat and CryoSat-2 radar freeboard retrieval over Antarctic sea ice, *The*  
992 *Cryosphere.*, 10, 1415-1425, doi: 10.5194/tc-10-1415-2016, 2016.

993 Skamarock, W. C., Klemp, J. B., Dudhia, J., Gill, D. O., Barker, D. M., Duda, M. G., Huang,  
994 X.-Y., Wang, W., and Powers, J. G.: A Description of the Advanced Research WRF Version  
995 3, NCAR Technical Note, 2008.

996 Stroeve, J. C., Markus, T., Maslanik, J. A., Cavalieri, D. J., Gasiewski, A. J., Heinrichs, J. F.,  
997 Holmgren, J., Perovich, D. K., and Sturm, M.: Impact of Surface Roughness on AMSR-E Sea  
998 Ice Products, *IEEE Transactions on Geoscience and Remote Sensing.*, 44, 3103-3117, doi:  
999 10.1109/TGRS.2006.880619, 2006.

1000 Warren, S. G., Rigor, I. G., Untersteiner, N., Radionov, V. F., Bryazgin, N. N., Aleksandrov,  
1001 Y. I., and Colony, R.: Snow Depth on Arctic Sea Ice, *Journal of Climate.*, 12, 1814-1829, doi:  
1002 10.1175/1520-0442(1999)012<1814:SDOASI>2.0.CO;2, 1999.

1003 Willatt, R. C., Giles, K. A., Laxon, S. W., Stone-Drake, L., and Worby, A. P.: Field  
1004 Investigations of Ku-Band Radar Penetration Into Snow Cover on Antarctic Sea Ice, *IEEE*  
1005 *Transactions on Geoscience and Remote Sensing.*, 48, 365-372, doi:  
1006 10.1109/TGRS.2009.2028237, 2010.

1007 Wingham, D. J., Francis, C. R., Baker, S., Bouzinac, C., Brockley, D., Cullen, R., De Chateau-  
1008 Thierry, P., Laxon, S. W., Mallow, U., Mavrocordatos, C., Phalippou, L., Ratier, G., Rey, L.,  
1009 Rostan, F., Viau, P., and Wallis, D. W.: CryoSat: A mission to determine the fluctuations in  
1010 Earth's land and marine ice fields, *Advances in Space Research.*, 37, 841-871, doi:  
1011 10.1016/j.asr.2005.07.027, 2006.

1012 Worby, A. P., Geiger, C. A., Paget, M. J., Woert, M. L. V., Ackley, S. F., and DeLiberty, T.  
1013 L.: Thickness distribution of Antarctic sea ice, *Journal of Geophysical Research: Oceans.*, 113,  
1014 C05S92, doi: 10.1029/2007JC004254, 2008a.

1015 Worby, A. P., Markus, T., Steer, A. D., Lytle, V. I., and Massom, R. A.: Evaluation of AMSR-  
1016 E snow depth product over East Antarctic sea ice using in situ measurements and aerial  
1017 photography, *Journal of Geophysical Research: Oceans.*, 113, C05S94,  
1018 doi: 10.1029/2007JC004181, 2008b.

1019 Wu, X., Budd, W. F., Lytle, V. I., and Massom, R. A.: The effect of snow on Antarctic sea ice  
1020 simulations in a coupled atmosphere-sea ice model, *Climate Dynamics.*, 15, 127-143, doi:  
1021 10.1007/s003820050272, 1999.

1022

1023

1024

1025